DOI: https://doi.org/10.14311/TPFM.2025.033

ON DYNAMICS OF THE WAKE BEHIND A WALL MOUNTED FINITE-LENGTH CYLINDER

V. Uruba[1, 2], P. Prochazka[1]

[1] Institute of Thermomechanics of the Czech Academy of Sciences, Dolejškova 5, 182 00 Praha 8, CR

[2] Faculty of Mechanical Engineering, Department of Power System Engineering, Universitní 8, 301 00 Plzeň, CR

Abstract

Dynamics of the wake behind a finite-length circular cylinder with an aspect ratio 2 is to be studied experimentally. The cylinder, mounted perpendicular to a ground plane, was exposed to a cross-flow with a thin boundary layer developed on the wall. The Reynolds number was 9700. The time-resolved Particle Image Velocimetry technique was used to investigate the dynamics of the wake in two planes parallel to the flow. Particular attention was paid to tip vortices, Kármán-like vortices and arch vortex dynamics in the near wake. Several kinds of vortex streets in the wake were identified and studied.

Keywords: circular cylinder, finite length, wake, dynamics, 3D structure

1 Introduction

The study of fluid flow around an infinitely long circular cylinder in cross-flow is a fundamental topic in fluid dynamics. This canonical case is characterized by the periodic shedding of vortices, known as the von Kármán-Bénard vortex street. Numerous experimental investigations and numerical simulations have explored this phenomenon extensively (e.g., [1-5]).

For this case the wake exhibits a fundamental shedding frequency. The dimensionless frequency, known as the Strouhal number Sr:

$$\mathrm{Sr} = \frac{f \cdot D}{U_e}, \quad (1)$$

where f is the shedding frequency, D is the cylinder diameter, and U_e is the freestream velocity. Across a broad range of Reynolds numbers higher than 200, the Strouhal number is typically about 0.2. The Reynolds number Re is defined as follows:

$$\mathrm{Re} = \frac{U_e \cdot D}{\nu}, \quad (2)$$

where U_e is the freestream velocity, D is the cylinder diameter and ν is kinematic viscosity.

However, in practical scenarios, cylinders have finite lengths, which significantly alter the flow characteristics. The influence of the finite length can be described by the aspect ratio AR:

$$\mathrm{AR} = \frac{L}{D}, \quad (3)$$

where L is the cylinder's length and D its diameter. Examples of finite-length cylinders include components in turbomachinery, structural elements in architecture, and various flow obstacles.

This study focuses on the wake dynamics of a finite-length circular cylinder. Despite its practical importance, the flow behaviour around finite cylinders are less thoroughly investigated compared to their infinite counterparts. However, we could find some experimental studies (e.g. [6-8]) as well as a few numerical simulations (e.g. [9, 10]). In most studies, only time-mean topology is presented, the dynamical aspects are not addressed. There are some exceptions as [11, 12] in mathematical simulations or our preliminary experimental study [13].

It has been shown that cylinders with AR > 5 exhibit wake behaviour similar to infinite cylinders, albeit with noticeable three-dimensional effects influenced by strong end effects. However, shorter cylinders AR < 5 demonstrate qualitatively different flow structures. Research suggests that for cylinders with aspect ratios below a critical value (AR_{crit}, reported between 2 and 6), the vortex shedding transitions from the anti-symmetric von Kármán type to a symmetric arch-type pattern. Subcritical aspect ratios are characterized by parallel vortex shedding in the wake, with tip vortices and base vortices emerging due to the interaction of three-dimensional flow structures. Tip vortices are formed near the cylinder's free ends, while base vortices result from a strong downwash effect. Additionally, a horse-shoe vortex can arise from the interaction between the wall boundary layer and the cylinder. Schematic view of the subcritical aspect ratio cylinder wake is shown in Fig. 1, however only time-mean view (from [8]). The Kármán-like vortex street is not depicted here.

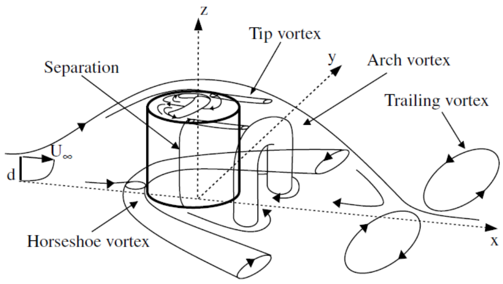

Figure 1: Schematic view of the time-averaged flow topology of the wake behind a finite-length cylinder (not to scale) - [8].

In this work, some aspects of the wake dynamics of this flow-field is to be addressed.

2 Description of Experiment

The existing blow-down facility located in the laboratory of the Institute of Thermomechanics, Academy of Sciences of the CR was used.

2.1 Experimental Set-Up

The test section is equipped with impermeable walls, the cross-section is 250 x 250 mm^2. The cylinder of diameter $D = 30$ mm and length 60 mm was attached to the test section wall close to its entrance, about 60 mm behind the contraction. The blockage of the cross-section by the model is less than 3 %. The boundary layer on the walls upstream the cylinder is very thin due to contraction located just upstream, its thickness is about a few millimeters (2-3 mm). The in-flow velocity was $U_e = 5$ m/s, resulting Reynolds number based on cylinder diameter was about 9.7 thousand. The dimensionless Cartesian coordinate system is introduced in Fig. 1 with origin in the cylinder bottom center, the streamwise direction is x, z is the cylinder axis, all distances are enumerated in the cylinder diameter multiples. So, the cylinder length is 2, which is the aspect ratio.

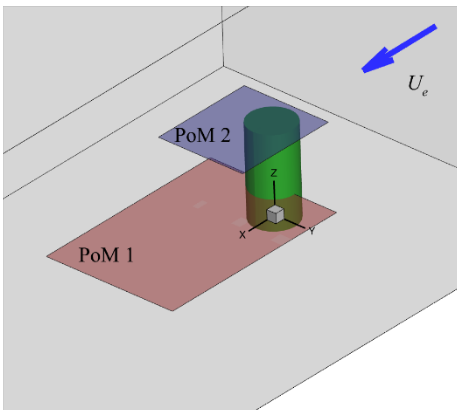

Figure 2: Experimental setup, PoM 1 in red, PoM 2 in blue.

The two Planes of Measurement (PoM) were chosen to study the wake dynamics to capture the wake 3D structure. Both are parallel to the cylinder bottom, z = const. The first PoM 1 is located relatively close to the cylinder bottom, 0.667 D above it, which corresponds to 1/3 of the cylinder height, i.e. $z = 0.667$, representing the wake behind the cylinder itself. The second PoM 2 covers the flow just above the cylinder top, z = 2.167. The PoM 1 is chosen to study dynamics of the arch vortex and Kármán-like vortex street, while PoM 2 is located in the tip vortex region.

2.2 Measurement Technique

The velocity vector fields were measured using Particle Image Velocimetry (PIV) method. The measurement apparatus consists of a laser and a CMOS camera by Dantec Company. The laser is New Wave Pegasus, Nd:YLF double head with wavelength of 527 nm, with maximal frequency 10 kHz and shot energy of 10 mJ (for 1 kHz), thus the corresponding power is 10 W per one head. The camera VEO 410 with resolution of 1 280 x 800 pixels is able to acquire double snaps with frequency up to 2500 Hz (full resolution), the internal memory is 16 GB evolving for storage 4 000 double-snapshots. The data were acquired and post-processed using the DynamicStudio and Tecplot software.

The PIV measurement was performed in the two PoMs – see Fig. 1. Statistics were evaluated from data acquired with frequency 100 Hz, 1 000 double-snapshots representing 10 s in real time. The dynamical measurement data consists of 4 000 double-snapshots acquired with frequency 2 kHz, thus representing 2 s of real time. The Safex generator of particles in the form of oil droplets was used, the mean diameter of the particles was 1 μm.

Only in-plane velocity components u and v in x and y directions were evaluated.

2.3 Analysis Methods

All evaluated quantities are to be presented in dimensionless forms. All lengths are given in multiples of D and velocities in multiples of the U_e.
The classical statistical analysis has been performed. Mean velocity fields were evaluated as well as the Turbulent Kinetic Energy (TKE) distributions. In the 2D representation the following definition of the dimensionless TKE was used:

$$\text{TKE} = \frac{\overline{u^2} + 2\overline{v^2}}{2U_e^2}\,, \tag{4}$$

where u is streamwise velocity fluctuation (x-component), v is spanwise velocity fluctuation (y-component), $\overline{}$ is average operation and U_e is the freestream velocity.

The Oscillation Pattern Decomposition (OPD) method has been used to study the flow-field dynamics, see [14]. The OPD method provides a series of OPD modes, each OPD mode is characterized by the topology in complex form (consisting of real and imaginary parts), frequency and attenuation of the pseudo-periodic (oscillating) behavior. The fluctuations are expected in the form of cyclostationary process, when the real and imaginary topology appear in frequency of a mode quarter period, first positive and then negative velocity distributions. The attenuation or amplitude decay is described by so called e-folding time representing the mean time period of the mode amplitude decay by factor "e". The other decay characteristic is the dimensionless "periodicity" p which expresses the e-folding time in multiples of periods of the OPD mode defined by its frequency:

$$p = \tau_e f\,, \tag{5}$$

here p is periodicity, τ_e is e-folding time and f is the mode frequency. The periodicity could be considered as a measure of the mode stability level and thus "importance".

3 Results

First, statistical characteristics representing time-averaged velocity field is to be shown. Then, dynamical structures are to be presented.

3.1 Statistics

In the PoM 1 close to the bottom wall, the mean-flow pattern is similar to this behind infinite-length cylinder including back-flow region located just behind the cylinder (confirm e.g. [3]).

In Fig. 3 the mean velocity characteristics in the PoM 1 are shown. In Fig. 3a, there is velocity vector-field with vector lines added arbitrarily. In Figs. 3b and 3c there are mean streamwise velocity component and TKE distributions, respectively. The white line represents border of back-flow region defined by negative U, it is attached to cylinder. The whole wake is dominated by elevated dynamic activity with maximum close to the rear part of the back-flow region.

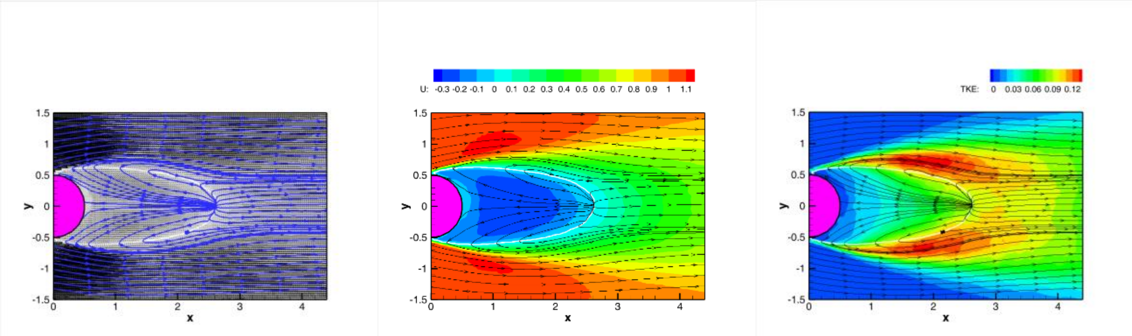

(a) (b) (c)

Figure 3: PoM 1 mean velocity vector-field (a), mean streamwise velocity component distribution (b) and TKE distribution (c).

Please note that no portal vortex could be detected in the time-averaged picture in the PoM 1.
In Fig. 4 the vector field of mean velocities distribution in the PoM 2 just above the cylinder is shown. Silhouette of the cylinder is depicted by broken white line, flow passes above the cylinder.

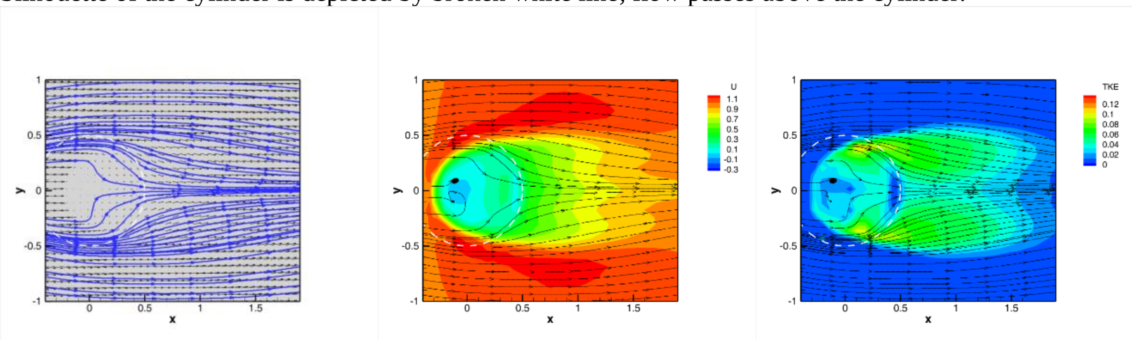

(a) (b) (c)

Figure 4: PoM 2 mean velocity vector-field (a), mean streamwise velocity component distribution (b) and TKE distribution (c).

Obviously, there is no back-flow region in the PoM 2, this is clear from Fig. 4b, where streamwise velocity component distribution is shown. Above the cylinder, there is low, but positive, velocity region. The flow dynamics represented by TKE is not so profound in the PoM 2.
To have a good comparison of differences between the PoMs 1 and 2, the identical colour scales are kept in Figs. 3 and 4.

3.2 OPD Analysis PoM 1

The spatio-temporal data analysis was applied in both PoMs. The spectrum showing modes frequency and periodicity will be shown first. Then, modes topology, real and imaginary parts, are to be presented. Three topologies are to be shown. First real and imaginary parts with corresponding velocity vector fields and vector-lines added in arbitrary manner. The colour represents vorticity, red positive, blue negative. Only topology is presented, so no scales are provided. The last topology shows schematically path of vortices centres movement in time for sampling a quarter of corresponding mode period. Point 0 shows origin of the vortex, higher numbers indicates time in multiples of the period. Thus, e.g. point 4 shows position of the vortex core originating in the point 0 for the time equal to 1 period.
In Fig. 5 the spectrum of data acquired in the PoM 1 is shown.

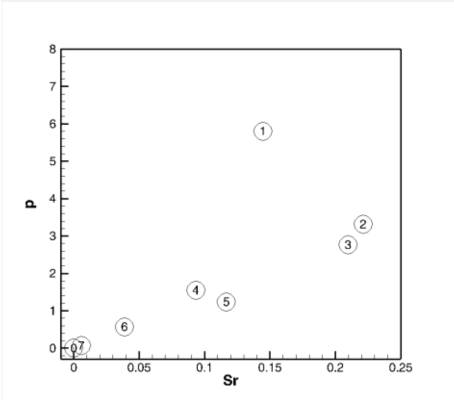

Figure 5: OPD spectrum in PoM 1.

The dominant OPD mode 1 is characterized by Strouhal number around 0.15, while two less dominant modes 2 and 3 has Strouhal number close to 0.2, which is typical for vortex Kármán street for long cylinder. The mode OPD 1 is represented by system of corotating vortex couples of the same orientation convected by the flow appearing alternatively with positive and negative vorticity. In Fig. 6 real (a) and imaginary (b) topologies are shown, we could detect 3 stages of the vortices in real topology and 2 stages in imaginary one. In Fig. 6c the evolution scheme of the vortex couple is shown tracking the vortices centres for phases during a period. Point 0 labels origin of the vortex, other points show positions of the vortex in a given multiple of the period.

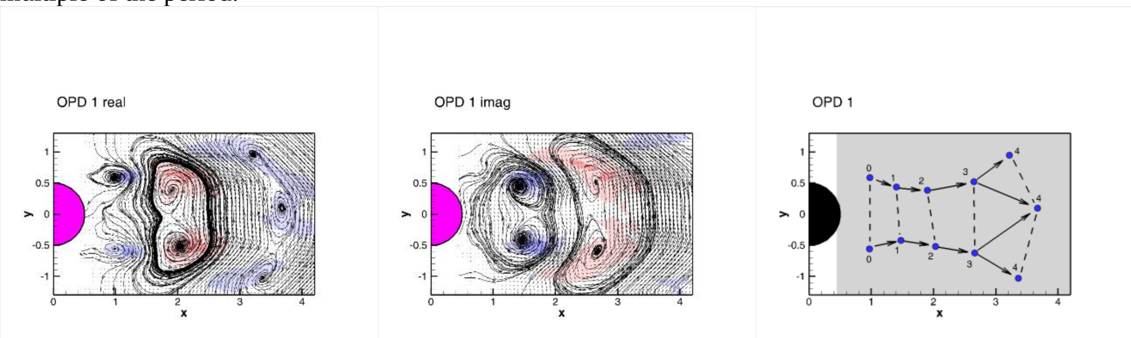

(a) (b) (c)

Figure 6: PoM 1, OPD mode 1, real (a) and imaginary (b) parts and evolution scheme (c).

The appearance of the cyclostationary topology begins with real (RE) for the 0 phase. In quarter of period follows the imaginary (IM), then -RE for half period, -IM for three quarters and again RE:

$$\mathrm{RE} \to \mathrm{IM} \to -\mathrm{RE} \to -\mathrm{IM} \to \mathrm{RE}\,. \qquad (6)$$

Let us follow the negative vorticity vortex couple in position $x \approx 1$ on RE. The displacement of this structure during one period is shown in Fig. 6c, where positions of vortices during one period is shown. The phase 0 means the first detectable position of the structure. The next positions 1-4 represent evolution in quarters of period (i.e. ¼, ½, ¾ and 1 period). Please note that the vortex couple is instable and splits in the end of period (phase 4 quarters) into 3 corotating vortices.

This topology could be related to the dynamics of the arch-vortex structures, which do not appear in averaged topologies (confirm Fig. 3).

The OPD mode 2 is presented in Fig. 7. This mode is dominated by contrarotating vortical couples drifted by the stream. The field of view contains of 7(8) quarters of period starting with the first appearance close behind the cylinder (phase 0).

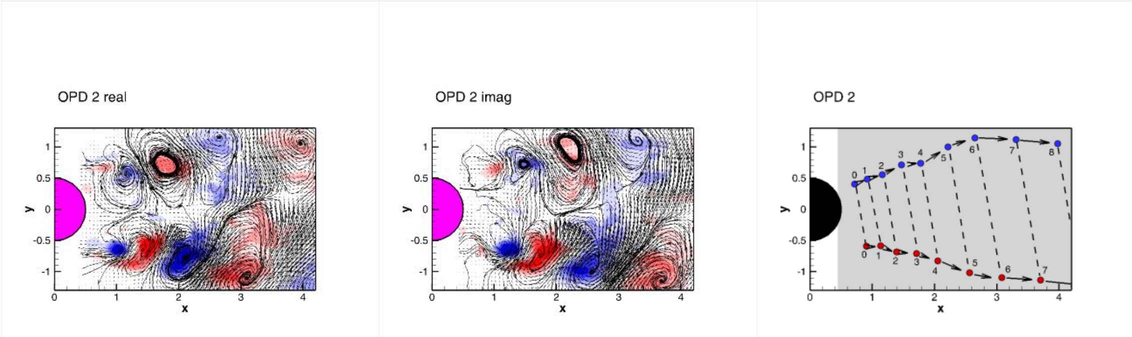

(a) (b) (c)

Figure 7: PoM 1, OPD mode 2, real (a) and imaginary (b) parts and evolution scheme (c).

The topology of the mode OPD 2 is similar to vortex Kármán street for long cylinder, however it is less regular. The mode OPD 3 is of a very similar frequency and topology, the important difference is in orientation of the vortices in couple – here they are corotating. The topology of the mode OPD 3 is in Fig. 8.

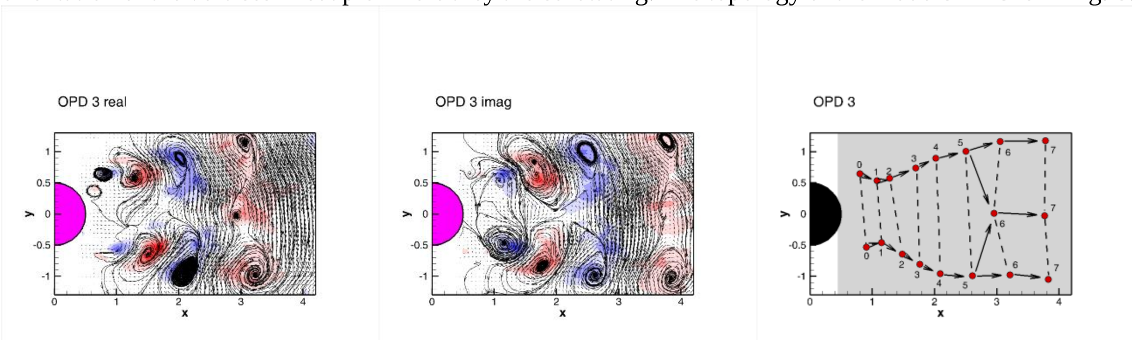

(a) (b) (c)

Figure 8: PoM 1, OPD mode 3, real (a) and imaginary (b) parts and evolution scheme (c).

The corotation configuration is less stable, it is subjected to instability in phase 5 quarters of period, where the couple is split into triplet.

The higher order OPD modes were analysed as well, however the topology is even less regular and the modes are decaying quicly in time, because of lower p.

The vortices are drifted by the stream accelerating in the streamwise direction. Their velocity as approximately identical for all OPD modes, it starts from about $0.25U_e$ in the point of origin 0, up to $0.5U_e$ in the end field of view, $x \approx 4$.

3.3 OPD Analysis PoM 2

The same analysis was applied to data from PoM 2 above the cylinder. In Fig. 9 the spectrum is presented.

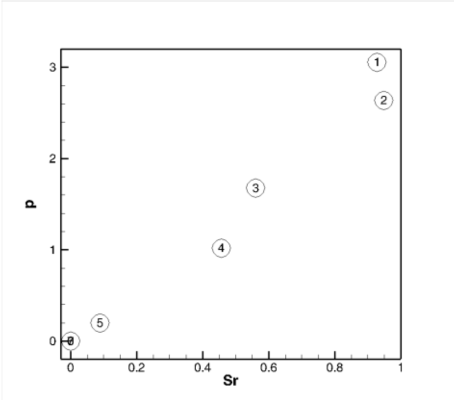

Figure 9: OPD spectrum in PoM 2

The two most dominant OPD modes 1 and 2 are characterized by much higher frequency, Strouhal number is close to 1. In Fig. 10 the OPD modes 1 and 2 topologies are presented.

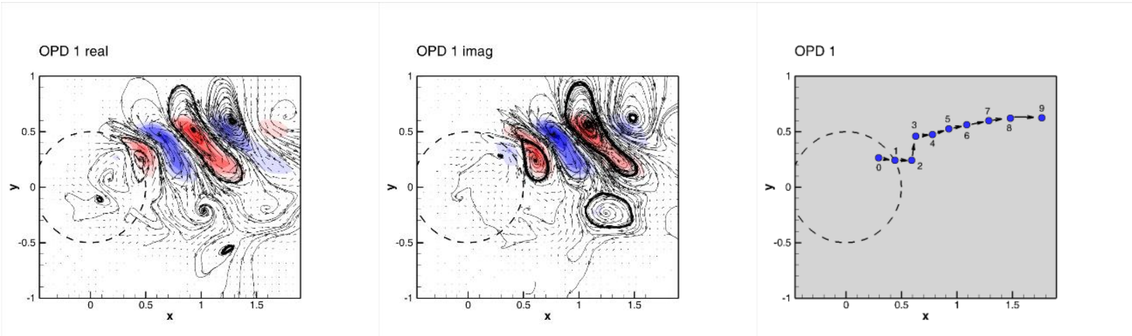

(a) (b) (c)

Figure 10: PoM 2, OPD mode 1, real (a) and imaginary (b) parts and evolution scheme (c).

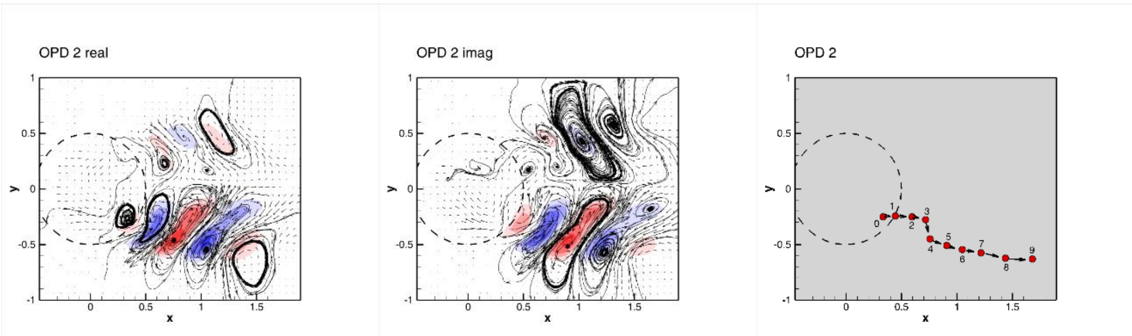

(a) (b) (c)

Figure 11: PoM 2, OPD mode 2, real (a) and imaginary (b) parts and evolution scheme (c).

The OPD modes 1 and 2 could be considered as complementary parts of a single dynamic process originating in a boundary layer on the cylinder top end. It generates kind of Kármán vortex street, but on much smaller virtual diameter resulting into higher shedding frequency. The OPD mode 1 represents the vortices in positive *y* half, while mode 2 the negative *y* half.
The vortex structures velocity in the PoM 2 is changing from about $0.5U_e$ on the vortex structures origin $x \approx 0.3$ (point 0) up to $0.75U_e$ close to $x \approx 1.5$.

4 Conclusions

The wake dynamical structure behind a finite-length circular cylinder with aspect ratio 2 mounted on a wall was studied experimentally in two PoMs for the Reynolds number 9700.

The wake behind the cylinder consists of various quasi-periodical vortical systems. The Strouhal number 0.15 corresponds to the strong corotating vortex pairs shed. The other two vortex systems with similar topology were identified, both with frequency close to 0.2 differing by internal structure. Both structures consist of vortex pairs drifted by the flow, one corotating, second contrarotating. Those structures are less regular than the first one. All these structures form dynamics of Kármán-like vortex street and arch vortex. No higher harmonics were identified behind the cylinder.

On the other hand, the wake dynamics just above the cylinder free end could be characterized by high frequency nonstationary tip vortices. They are represented by alternating vortex street of high frequency small vortices, Strouhal number approaches 1.

References

[1] von Kármán, T.: Aerodynamics. Columbus: McGraw-Hill (1954)

[2] Roshko, A.: On the development of turbulent wakes from vortex streets. *NACA Rep. 1191* (1955) pp. 801-825

[3] Williamson, C.H.K.: Vortex Dynamics in the Cylinder Wake, *Annu. Rev. Fluid. Mech.* vol. 28 (1996) pp. 477-539

[4] Garcia, B., Weymouth, G., Nguyen, V. & Tutty, O.: Span effect on the turbulence nature of flow past a circular cylinder. *J. Fluid Mech.* vol. 878 (2019) pp. 306-323

[5] Uruba, V., Procházka, P., Skála, V.: On the 3D Dynamics of the Wake Behind a Circular Cylinder, In: *Proceedings Topical Problems of Fluid Mechanics 2020*, Edited by D. Šimurda and T. Bodnár, (2020) pp. 240-248

[6] Norberg, C.: An experimental investigation of the flow around a circular cylinder: influence of aspect ratio, *J. Fluid Mech*., vol. 258 (1994) pp. 287-316

[7] Sumner, D., Heseltine, J.L., Dansereau, O.J.P.: Wake structure of a finite circular cylinder of small aspect ratio, *Experiments in Fluids* 37 (2004) pp. 720–730

[8] Pattenden, R.J., Turnock, S.R., Zhang, X.: Measurements of the flow over a low-aspect ratio cylinder mounted on a ground plate. *Exp. Fluids* 39 (2005) pp. 10–21

[9] Palau-Salvador, G., Stoesser, T., Frohlich, J., Kappler, M. & Rodi, W.: Large eddy simulations and experiments of flow around finite-height cylinders. *Flow Turbul. Combust*. 84 (2010) pp239–275.

[10] Krajnovic, S.: Flow around a tall finite cylinder explored by large eddy simulation, *J. Fluid Mech*., Vol. 676 (2011) pp. 294-317

[11] Saha, A. K.: Unsteady flow past a finite square cylinder mounted on a wall at low Reynolds number, *Comput. Fluids*, Vol. 88 (2013) pp. 599-615

[12] Amor, Ch., Pérez, J.M., Schlatter, P., Vinuesa, R. and Le Clainche, S.: Soft computing techniques to analyze the turbulent wake of a wall-mounted square cylinder, *Advances in Intelligent Systems and Computing* (2019) pp. 577–86

[13] Uruba, V., Procházka, P.: Dynamics of the Tip Vortices in the Wake Behind a Circular Cylinder of Finite Length, *MATEC Web of Conferences*, vol. 328 (2020) 05008

[14] Uruba V.: Near Wake Dynamics around a Vibrating Airfoil by Means of PIV and Oscillation Pattern Decomposition at Reynolds Number of 65 000, *Journal of Fluids and Structures*, vol. 55, (2015) pp. 372-383